J. Fluid Mech. (2010), *vol.* 655, *pp.* 198–216.
doi:10.1017/S0022112010000844

Vortex formation out of two-dimensional orifices

GIANNI PEDRIZZETTI†
D.I.C.A., Università di Trieste, P. le Europa 1, 34127 Trieste, Italy

(Received 28 July 2009; revised 9 February 2010; accepted 9 February 2010;
first published online 5 May 2010)

The understanding of the vortex formation process is currently driving a novel attempt to evaluate the performance of fluid dynamics in biological systems. The concept of formation time, developed for axially symmetric orifices, is here studied in two-dimensional flows for the generation of vortex pairs. The early stage of the formation process is studied with the single vortex model in the inviscid limit. Within this framework, the equation can be written in a universal form in terms of the formation time. The single vortex model properly represents the initial circular spiralling vortex sheet and its acceleration for self-induced motion. Then, an analysis is performed by numerical simulation of the two-dimensional Navier–Stokes equations to cope with the spatially extended vortex structure. The results do not show the pinch-off phenomenon previously reported for vortex rings. The two-dimensional vortex pair tends to a stably growing structure such that, while it translates and extends longitudinally, it remains connected to the sharp edge by a shear layer whose velocity is always about twice that of the leading vortex. At larger values of the Reynolds number the instability of the shear layer develops small-scale vortices capable of destabilizing the coherent vortex growth. The absence of a critical formation number for two-dimensional vortex pairs suggests further considerations for the development of concepts of optimal vortex formation from orifices with variable curvature or of a tapered shape.

1. Introduction

The blood flow in the human left ventricle is known to develop a vortical motion during the ventricular filling that should reduce energy dissipation and possibly facilitate the following ejection of blood into the primary circulation (Kilner *et al.* 2000; Pedrizzetti & Domenichini 2005). The presence of the intraventricular vorticity is central in the balance between flow and surrounding tissues; its quantification is driving novel attempts to improve understanding of cardiac diseases (Gharib *et al.* 2006; Hong *et al.* 2008), and to build synthetic models of the cardiac transvalvular flow (Korakianitis & Shi 2006).

The approach introduced in Gharib *et al.* (2006) for a potential vortex-based diagnosis of cardiac health is grounded on the concept of universal formation time introduced by Gharib, Rambod & Shariff (1998). This concept supports the existence of a limiting process during the vortex growth, that does not allow the vortex to retain its individuality for indefinitely long time. Its growth continues until the so-called formation time Vt/D, where V is the average velocity across the orifice, D its diameter, and t is time, is below a critical value; afterwards, the vortex stops growing

† Email address for correspondence: giannip@dica.units.it

and secondary vortices develop in its wake. Recent experimental studies with model ventricles also showed that when the duration of the flow across the mitral valve is about equal to the critical formation time the vortex thrust is maximized (Kheradvar & Gharib 2009). The transfer of this concept into the left ventricle suggests that a healthy filling flow should be such that the formation time is close to the critical value to optimize cardiac work and avoid generation of incoherent weakly turbulent cardiac flow. Nevertheless this transposition requires some care when dealing with a jet entering a chamber with a finite length; in this case the ratio between the jet length, proportional to Vt and the ventricular length, L (where $L \simeq 3$–$6D$), must also be considered. Actually, in the left ventricle, a jet with a formation time above the critical value may also correspond to a jet that reaches and splashes over the ventricular walls.

The existence of the critical formation number as a universal law emerging from vortex ring dynamics has been analysed and confirmed in a series of papers either based on numerical evidence (Rosenfeld, Rambod & Gharib 1998; Mohseni, Ran & Colonius 2001) or theoretical models (Mohseni & Gharib 1998; Shusser & Gharib 2000; see also Krueger 2008, for a different approach). In extreme synthesis, the forming vortex ring is continuously fed by the rolled-up shear layer separating from the orifice edge, therefore its circulation grows and the self-induced vortex translation velocity, proportional to circulation, increases as well (given that the core size grows very slowly, if the Reynolds number is high enough, and the ring diameter does not change significantly). The self-induced translation velocity of the vortex ring rises until it exceeds the velocity of the separating shear layer; at that point the newly separated vorticity cannot reach the vortex and eventually rolls up in its wake (Shusser & Gharib 2000). At this point the primary vortex detaches from the edge (pinch-off) and the dynamical interaction with the orifice decreases (Kheradvar & Gharib 2007). In one sentence, vortex ring pinch-off occurs when the velocity of the trailing jet (source flow) falls below the celerity of the leading vortex ring (Dabiri & Gharib 2005).

A similar analysis of the vortex formation process in two-dimensional systems, where a vortex ring is replaced by a symmetric vortex pair, has received less attention. Two-dimensional vortex pairs still present a self-induced velocity, therefore the basic concept at the base of the formation process could be analogous (M. Gharib & A. Kheradvar, 2009 personal communications). On the other side, two-dimensional vortex dynamics presents significant differences from axially symmetric systems, in particular it does not present the vortex stretching and enstrophy increase due to the radial displacement of circular vortex lines, and allows, roughly speaking, a less constrained vortex motion.

A two-dimensional model of the vortex formation process is also physically relevant for several applications; it may sometimes represent a more adequate approximation for the early flow across biological valves with tapering shape. However, despite the mentioned cardiac flow perspective, the present analysis is theoretical in nature and the potential relevance for biological applications is not discussed here. This study is only aimed at verifying whether the critical formation time concept applies or is modified for the formation of two-dimensional vortex pairs. The analysis is performed in the ideal condition of vortex formation after a diaphragm is placed between two infinitely extended chambers; this condition is well established for vortex ring formation and allows one to focus on the pure formation process without side effects. The only remaining connection with biological flows is represented by the value of the Reynolds number that, with the figures of cardiac orifices, ranges from values below 1000 (found in children) up to rare extremes of about 5000.

The roll-up of a single two-dimensional vortex sheet from a semi-infinite sharp edge is self-similar, because no external length scale exists (Rott 1956). It was studied by Pullin (1978) by an inviscid vortex sheet model, and by Luchini & Tognaccini (2002) by an accurate direct numerical simulation that also documented that the instability of the rolled-up shear layer (analogous to the Kelvin–Helmholtz instability for a plane vortex sheet) naturally occurs when the Reynolds number increases above a critical value there estimated as about 4500. The dynamics of a two-dimensional vortex pair generated by a piston pushing fluid out of an orifice was analysed by Blondeaux & De Bernardinis (1983), in the limit of high Reynolds number, by using the inviscid vortex method and experimental visualization. This work demonstrated the reliability of such an application of a model based on a single vortex method, often known as the Brown & Michael model (Brown & Michael 1954). It also showed that the separation and strength of the vortices strongly depend upon the time history of the piston motion although this dependence was not addressed and attention was focused on the formation of secondary vortices that develop when the piston is impulsively stopped. The two-dimensional impulsive vortex formation was studied numerically for the case of a sharp edge door opening in a straight channel (Pedrizzetti & Domenichini 2006). The process of vortex formation presented different regimes, from a short-time solution (Pedrizzetti 2005) to a fully separated self-similar wake that eventually develops secondary vortices behind the leading one. This was apparently due to the instability of the elongated shear layer and not to the pinch-off of the first vortex; nevertheless the vortex formation time was revealed as an appropriate variable to scale results obtained under different conditions.

An experimental study of the formation of a vortex dipole from an orifice is reported in Afanasyev (2006), there the pinch-off was not observed in any of the experiments. Those experiments – initially surprisingly also for the authors – showed that a critical formation time number does not exist in two dimensions; at least at the relatively low values (few hundred) of the Reynolds number investigated there. Experiments at higher Reynolds number, from 3400 to 7200, were performed by Hofmans (1998); those experiments were integrated by parallel numerical solutions using the vortex blob technique, and using the finite difference approximation of the Euler equations with artificial viscosity. The reported results (Hofmans 1998, chapter 3) actually show the detachment, apparently a sort of pinch-off, of the leading vortex pair. Such two-dimensional results, however, present two remarkable differences from their axially symmetric counterparts. First, the phenomenon starts from shear layer instability involving the entire vortex structure that becomes eventually incoherent (turbulent, in the experiment), and does not show the compact single vortex ring detaching and travelling away (pinch-off). Second, the velocity of the leading vortex pair remains always lower than the separating shear layer, therefore the detachment mechanism is not that of a vortex ring moving faster and away from the shear layer behind. In fact, the distance (in orifice size units) travelled by the vortex, that in axisymmetric flow is comparable to the formation time Vt/D, is here much lower (3–7 times). In addition, the formation time at the beginning of the shear layer instability ranges approximately from 60 to 90, figures not commensurable with the critical value (about 4) well established for vortex rings. In the same work (Hofmans 1998, chapter 4), an experiment in slightly different conditions shows a stable translating vortex pair at Reynolds number 1256.

The reason for these differences between vortex formation from a circular orifice and from a rectilinear opening remains an open issue. It has a theoretical interest

and represents a necessary preliminary step to approach vortex formation from three-dimensional orifices with variable curvature as is the case of natural valves.

The analysis is initially performed in the limit of infinite Reynolds number using the single vortex, Brown & Michael, model, a relatively simple mathematical framework that permits pursuing part of the study in analytical terms and highlighting some general phenomena in the early stage of the vortex formation process. The analysis is then performed, at finite Reynolds number, by numerical integration of the Navier–Stokes equations in order to progress under realistic conditions and accounts for the extended distribution of the separated vorticity.

2. Single vortex analysis

2.1. *Fundamentals*

Consider a two-dimensional incompressible flow across an orifice, indicating with an overline the dimensional quantities; let $2\overline{d}$ be the width of the orifice and $\overline{V}V(t)$ the average velocity at the opening, where $V(t)$ is the dimensionless velocity time profile and $t = \overline{t}\overline{V}/\overline{d}$ is the dimensionless time. The problem is treated from now onwards in dimensionless terms.

The orifice has two sharp edges at the coordinate points $z_e = \pm\mathrm{i}$ of the complex coordinate plane $z = x + \mathrm{i}y$. Using the conformal transformation $\zeta(z) = F(z)$, that for the case of a symmetric orifice in unbounded space is (see, for example, Lamb 1932, Art. 66)

$$\zeta = F(z) = \frac{2}{\pi}\log(\mathrm{i}z + \mathrm{i}\sqrt{z^2+1}) - \mathrm{i}, \qquad z = F^{-1}(\zeta) = -\mathrm{i}\cosh\left(\frac{2}{\pi}(\zeta + \mathrm{i})\right), \quad (2.1)$$

the physical plane is mapped onto a transformed plane, ζ, having the geometry of a rectilinear duct where the sharp edges are mapped on the opposite facing walls at $\zeta_e = \pm\mathrm{i}$.

In the limit of non-zero, vanishing viscosity the flow is assumed everywhere irrotational with the exception of two symmetric singular vortices, at $z_v(t)$ and $z_v^*(t)$, where * stands for complex-conjugate, of circulation $\Gamma(t)$ and $-\Gamma(t)$, respectively. The singular vortices represent a minimal model where the rolled-up vortex sheets separated from the sharp edges are concentrated at the vorticity centres (Brown & Michael 1954). The flow that satisfies the impermeability boundary conditions at the walls can be immediately evaluated in the transformed space where the complex potential is given by

$$W(\zeta, t) = V\zeta + \mathrm{i}\frac{\Gamma}{2\pi}\log\left\{\frac{\sin(\mathrm{i}\pi/4)(\zeta - \zeta_v)\sin(\mathrm{i}\pi/4)(\zeta - \zeta_v + 2\mathrm{i})}{\sin(\mathrm{i}\pi/4)(\zeta - \zeta_v^*)\sin(\mathrm{i}\pi/4)(\zeta - \zeta_v^* + 2\mathrm{i})}\right\}, \quad (2.2)$$

and $\zeta_v = F(z_v)$ is the position of the vortex in the transformed space. Potential (2.2) accounts for a periodic vortex pair along the imaginary axis that satisfies the boundary condition on either wall. The flow potential in the physical space is $W(z) = W(\zeta(z))$, and the complex-conjugate velocity at a generic point z is $v^*(z) = \mathrm{d}W/\mathrm{d}z = \mathrm{d}W/\mathrm{d}\zeta\ F'$ where, from (2.2),

$$\frac{\mathrm{d}W}{\mathrm{d}\zeta} = V + \frac{\Gamma}{4}\left\{\cot\frac{\mathrm{i}\pi}{2}(\zeta - \zeta_v^*) - \cot\frac{\mathrm{i}\pi}{2}(\zeta - \zeta_v)\right\}. \quad (2.3)$$

The dynamic system specification seeks the evolution of vortex position $z_v(t)$ and intensity $\Gamma(t)$ for a given flow $V(t)$ across the orifice. The vortices are advected by

the local velocity in terms of the zero-force condition to account for the growing circulation and the fact that they are not free vortices but they are a simplified representation of a rolling-up vortex sheet attached to the sharp edge (Brown & Michael 1954; Rott 1956)

$$\Gamma \frac{\mathrm{d}z_v}{\mathrm{d}t} + (z_v - z_e)\frac{\mathrm{d}\Gamma}{\mathrm{d}t} = \Gamma v(z_v). \tag{2.4}$$

The computation of the local velocity, $v(z)$, appearing in (2.4), at the vortex position is calculated by the Routh rule (Routh 1881) to properly eliminate the vortex self-induction in physical space

$$\begin{aligned} v^*(z_v) &= \lim_{z\to z_v} \frac{\mathrm{d}}{\mathrm{d}z}\left\{ W - \frac{\mathrm{i}\Gamma}{2\pi}\log(z - z_v)\right\} \\ &= \lim_{z\to z_v} \frac{\mathrm{d}}{\mathrm{d}\zeta}\left\{ W - \frac{\mathrm{i}\Gamma}{2\pi}\log(\zeta - \zeta_v)\right\} F' + \frac{\mathrm{i}\Gamma}{2\pi}\lim_{z\to z_v}\frac{\mathrm{d}}{\mathrm{d}z}\log\left(\frac{\zeta-\zeta_v}{z-z_v}\right) \\ &= \left\{ V + \frac{\Gamma}{4}\cot\frac{\mathrm{i}\pi}{2}(\zeta_v - \zeta_v^*)\right\} + \frac{\mathrm{i}\Gamma}{4\pi}\frac{F''}{F'}\bigg|_{z_v}. \end{aligned} \tag{2.5}$$

In (2.5) the fact that the periodic extension of the self-induction term is zero by symmetry has also been used, and the second limit is evaluated by expanding the numerator of the logarithm argument in a Taylor series.

In the limit of a viscous flow with vanishing viscosity the boundary layer is everywhere of zero thickness and detaches from the sharp edge to ensure the physical requirement, known as the Kutta condition, that velocity must be finite at the sharp edge. The transformation F' is singular at the sharp edges and the Kutta condition reads $\mathrm{d}W/\mathrm{d}\zeta|_{z_e} = 0$ that becomes, using (2.3),

$$\Gamma = 4V\frac{\cos(\mathrm{i}\pi/2)\ \zeta_v \cos(\mathrm{i}\pi/2)\zeta_v^*}{\sin(\mathrm{i}\pi/2)(\zeta_v - \zeta_v^*)}. \tag{2.6}$$

The evolution of the position and circulation of the separated vortex pair can thus be performed by (2.4)–(2.6).

2.2. *Self-similar equation*

The mathematical formulation can be progressed further to include the Kutta condition (2.6) implicitly into evolutionary equation (2.4). Time differentiation of (2.6)

$$\frac{\mathrm{d}\Gamma}{\mathrm{d}t} = \left[\frac{\mathrm{d}\Gamma}{\mathrm{d}\zeta_v}F'(z_v)\right]\frac{\mathrm{d}z_v}{\mathrm{d}t} + \left[\frac{\mathrm{d}\Gamma}{\mathrm{d}\zeta_v}F'(z_v)\right]^*\frac{\mathrm{d}z_v^*}{\mathrm{d}t} + \frac{\Gamma}{V}\frac{\mathrm{d}V}{\mathrm{d}t}$$

shows that it depends on the evolution of the vortex position and its complex-conjugate. Placing (2.4) in a system with its complex-conjugate version, inserting the expression for $\mathrm{d}\Gamma/\mathrm{d}t$, and solving for $\mathrm{d}z_v/\mathrm{d}t$ eventually leads to

$$\frac{\mathrm{d}z_v}{\mathrm{d}t} = \frac{[\mathrm{d}\Gamma/\mathrm{d}\zeta_v\, F']^*(z_v - z_e)^* v - [\mathrm{d}\Gamma/\mathrm{d}\zeta_v\, F']^*(z_v - z_e)v^* + \Gamma v}{[\mathrm{d}\Gamma/\mathrm{d}\zeta_v\, F']^*(z_v - z_e)^* + [\mathrm{d}\Gamma/\mathrm{d}\zeta_v\, F'(z_v)](z_v - z_e) + \Gamma}; \tag{2.7}$$

with F' and v the values at the vortices $F'(z_v)$ and $v(z_v)$ are intended and Γ is the function of z_v given by (2.6).

Inspection of (2.7), and of the functions of z_v contained therein ((2.5) and (2.6)), shows that it can be normalized with respect to the external forcing $V(t)$. Define the

normalized circulation and the normalized velocity

$$\gamma = \frac{\Gamma}{V}, \qquad u(z_v) = \frac{v(z_v)}{V}$$

both functions of z_v only (see (2.5) and (2.6)) that do not contain a dependence on $V(t)$ anymore. The formation time

$$\tau = \frac{1}{2}\int_0^t V(t)\,\mathrm{d}t \tag{2.8}$$

naturally arises (the factor $1/2$ is due to normalization with the orifice size, equal to two dimensionless units, that is included to agree with the definition in the literature), and it permits rewriting of (2.7) in terms of the normalized variables

$$\frac{\mathrm{d}z_v}{\mathrm{d}\tau} = 2\frac{[\mathrm{d}\gamma/\mathrm{d}\zeta_v\, F']^*\,(z_v - z_e)^* u - [\mathrm{d}\gamma/\mathrm{d}\zeta_v\, F']^*\,(z_v - z_e) u^* + \gamma u}{[\mathrm{d}\gamma/\mathrm{d}\zeta_v\, F']^*\,(z_v - z_e)^* + [\mathrm{d}\gamma/\mathrm{d}\zeta_v\, F'(z_v)]\,(z_v - z_e) + \gamma}. \tag{2.9}$$

Equation (2.9) is an evolutionary function for z_v, where the right-hand side does not depend on the external forcing $V(t)$. It is therefore a universal equation for the formation of a vortex pair. The solution $z_v(\tau)$ includes implicitly all the solutions corresponding to different profiles $V(t)$ that are recovered simply by a proper re-scaling of time (2.8).

Equation (2.9) also shows that vortex formation can be described in terms of τ only; it therefore provides a mathematical support for the fundamental significance of the formation time and, at least for a given geometry, for the universality of vortex formation events independently from the details of $V(t)$.

2.3. *Computational results*

Equation (2.9) can be integrated numerically by standard techniques. It presents a difficulty just at the initial condition, $z_v(0) = z_e$, where it is square root singular. However, in the limit $z_v \to z_e$, the equation can be integrated analytically to give the asymptotic small-time solution

$$z_v(t) = \pm \mathrm{i} + \frac{2^{2/3}}{\pi}\tau^{2/3} \tag{2.10}$$

that is used to define the initial evolution for numerical integration (numerically, to integrate the first time step). Equation (2.9) is integrated with an explicit second-order method, and adaptive time-step, and results have been verified to be independent of the time resolution; computational time is negligible and time steps much smaller than required are employed.

The time profile of the general solution is reported in figure 1, and the corresponding flow field at two instants is shown in figure 2. The vortex structure initially evolves with self-similar solution (2.10). Then, the external length scale due to the orifice size comes into play and the self-induced motion of the vortex pair becomes significant. While the vortex pair moves away from the orifice its circulation must grow to enforce the Kutta condition; the growth of circulation is progressively faster than in the case of a single vortex (when it would be self-similar, $\gamma \sim \tau^{1/3}$) because the self-induced velocity takes the pair further away from the edge, requiring, in turn a higher circulation to satisfy the Kutta condition. This process leads to a continuously accelerating vortex motion and a more than exponential divergence.

This model is an approximation for the early stage of the vortex formation process. The concentration of the entire wake into a single vortex represents an appropriate

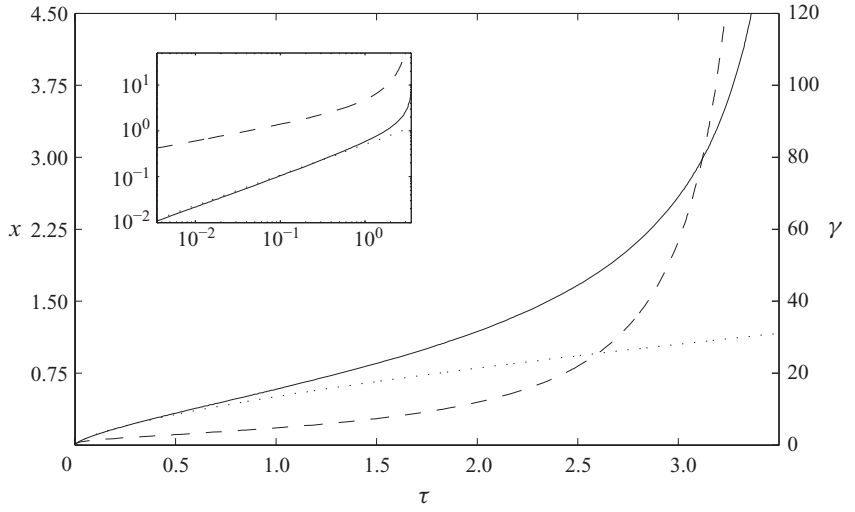

FIGURE 1. Vortex formation from a symmetric orifice. Time evolution of the normalized vortex x-position (continuous line) and of the normalized circulation $\gamma(\tau)$ (dashed line), the dotted line is short-time asymptotic (2.10). The inset shows the same graph with logarithmic scales.

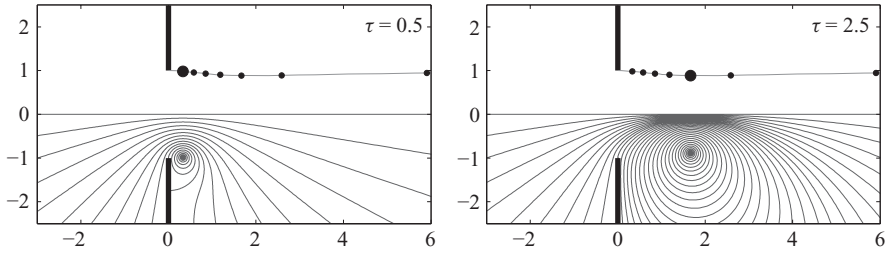

FIGURE 2. Vortex formation from a symmetric orifice. Streamlines (lower half) and vortex trajectory (upper half) corresponding to $\tau = 0.5$ and $\tau = 2.5$. Streamfunction levels are equispaced from 0 to 1 and logarithmic-spaced for higher values to cope with the singular behaviour. The black circles on the vortex trajectories are spaced by $\Delta\tau = 0.5$, the larger circle indicates the current position.

model of a rolling-up vortex sheet until it maintains the shape of an approximately circular spiral. In the present realizations, the separated vortex layer is initially expected to roll-up into a circular spiral; afterwards the vortex deforms while it translates downstream remaining attached to the sharp edge with minimal transversal displacement. Therefore, the singular model becomes a less realistic representation of the separated wake as its distance from the orifice becomes comparable with the size of the orifice itself.

This limitation (say, the requirement that the vortex distance does not exceed, at most, the orifice size) occurs well before the final accelerated phase, therefore the single vortex model contains the basic elements of the early vortex formation process, witnessing its universal character, the significance of the formation time concept, and the initial role of the self-induction. On the other side it does not permit the drawing of any conclusion on the following phenomena, including the existence or not of the pinch-off process, that are required to properly account for the finite distribution of vorticity.

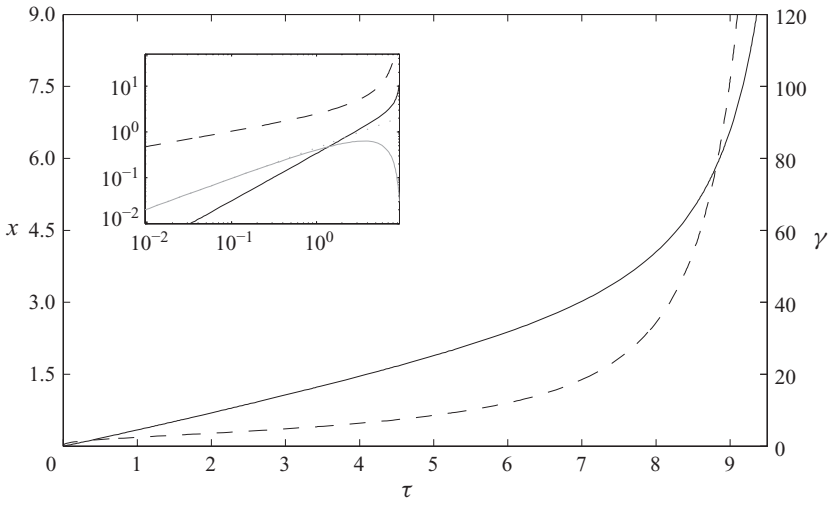

FIGURE 3. Vortex formation at the exit of a semi-infinite duct. Time evolution of the normalized vortex x-position (continuous line) and of the normalized circulation $\gamma(\tau)$ (dashed line). The inset shows the same graph with logarithmic scales and, in grey scale, the evolution of the vortex y-position with the dotted line corresponding to the short-time solution.

In the axially symmetric systems, the formation process of vortex rings, and the value of the critical formation time, were shown to be little influenced by the velocity spatial profile at the orifice or by its actual geometry (Rosenfeld *et al.* 1998). It depends on the strength and velocity of the shear layer (both proportional to the velocity V) that give the rate of circulation growth. As a final contribution from the singular vortex model, the influence of the orifice geometry in the early phase of the two-dimensional formation process is verified. This is achieved by simply changing the conformal map in (2.9) with that of a two-dimensional semi-infinite duct given by (see, for example, Lamb 1932, Art. 66)

$$z = F^{-1}(\zeta) = \zeta + \frac{1}{\pi}(1 + \exp(\pi\zeta)) ;$$

whose corresponding small-time asymptotic solution is

$$z_v(t) = \pm \mathrm{i} \pm \mathrm{i}\frac{2^{1/2}}{\pi}\tau^{2/3}.$$

This geometry differs in the angle of the tube prior to the orifice that was nominally zero in the diaphragm and is $\pi/2$ here. Consequently the small-time solution has only the imaginary component and tends initially to separate the pair of vortices. These are two extreme cases and should represent bounds for all intermediate orifice shapes.

The general solution is reported in figure 3 (compare with figure 1). The general behaviour of vortex formation is confirmed: vortices initially slowly move forward, then the self-induction effect leads to a rapidly accelerating motion and circulation growth. However, the process is significantly slower in this case. This result evidences that geometry does not affect the phenomenon qualitatively, however, differently from the axisymmetric case, it has a relevant influence on the quantitative assessment of timings of two-dimensional vortex formation.

3. Numerical simulations analysis

3.1. *Numerical method*

The vortex formation process from a sharp orifice, corresponding to geometry (2.1), is here studied numerically by solution of the two-dimensional Navier–Stokes equation written in the vorticity–streamfunction, $\omega - \psi$, formulation in physical space

$$\frac{\partial \omega}{\partial t} + \frac{\partial \psi}{\partial y}\frac{\partial \omega}{\partial x} - \frac{\partial \psi}{\partial x}\frac{\partial \omega}{\partial y} = \frac{2}{Re}\nabla^2\omega; \tag{3.1}$$

with the Poisson relation $\nabla^2\psi = -\omega$, and the Reynolds number defined by $Re = \overline{V}2\overline{d}/\nu$, ν being the kinematic viscosity. The domain extends in the range $-\infty < x < +\infty$ and $-\infty < y \leqslant 0$, $y = 0$ being a symmetry axis. A semi-infinite no-slip wall of zero thickness is located on the plane $x = 0$ extending infinitely downwards from the sharp edge at $y = -1$.

Cartesian coordinates are made discrete using second-order centred finite differences with constant grid spacing. In order to facilitate the imposition of the boundary conditions on the finite domain, the streamfunction is subdivided into the sum of the known irrotational contribution $\psi_0 = V(t)\mathcal{I}(\zeta)$, where $\mathcal{I}(\zeta)$ is the imaginary part of ζ given by map (2.1), and an unknown correction ψ_1, such that the Poisson equation is solved for the correction only: $\nabla^2\psi_1 = -\omega$. At the finite far ends of the numerical domain the condition of zero second normal derivatives is imposed either on the vorticity or the correction streamfunction. Symmetry conditions, $\psi_1 = 0$, $\omega = 0$, are set on $y = 0$. The streamfunction is continuous across the no-slip wall and constant on it, where the correction streamfunction is set to zero. The vorticity is discontinuous across the wall, and is evaluated by the Poisson relation evaluated at first order on the two sides of the wall, with the additional no-slip condition of zero normal derivative of the complete streamfunction. Given that the wall has zero thickness, an auxiliary vorticity variable is used to account for the different values at the two sides of the wall. Time evolution is performed with a second-order Adams–Bashforth scheme and constant time step.

The same code has been used in previous works (see for example, Pedrizzetti & Domenichini 2006; Pedrizzetti & Domenichini 2007) from which this specific version has been extracted after simplification. Further technical details can be found therein. An additional validation has been performed here by comparing the early flow near one of the orifice edges with the self-similar solution behind a semi-infinite wedge. The numerical solution of that problem contains the critical issue of lacking a fixed reference length scale; the only scale is that of the developing spiral and increases with time. This issue is also partly present here, at the early times of the orifice flow, and the validation is aimed at verifying that the unavoidable, lower resolution during the initial stages of shear layer separation does not influence the subsequent flow development. The numerical solution of that problem was obtained by Luchini & Tognaccini (2002) where self-similar time-varying coordinates, scaled with $2\sqrt{\nu t}$, are introduced to ensure that the accuracy remains approximately constant during evolution. The comparison with the accurate numerical results of Luchini & Tognaccini (2002) has been performed in the more challenging case of impulsively started flow; the period before the appearance of shear layer instability is considered here, because the timing of the appearance of such later instabilities – even when the numerical solution was unstable – may depend on the numerical perturbations intrinsic to the software and machine precision. Two examples of the solution are reported in figure 4, for two different combinations of parameters corresponding to

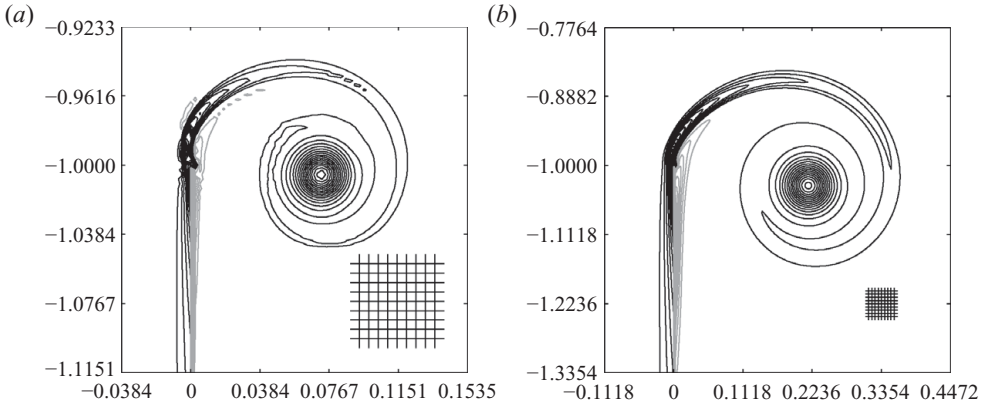

FIGURE 4. Close-up view of the numerical solution of the orifice flow near one edge, for comparison with the results from Luchini & Tognaccini (2002) for an impulsively started flow (*a*) $Re = 6800$, $t = 0.1$; (*b*) $Re = 8000$, $t = 0.5$. Both cases would correspond to the same self-similar solution in the case of an infinite wedge, with a scaled Reynolds number $Re_s = 2743$ (Luchini & Tognaccini 2002, figure 2*b*); the scaled length $2\sqrt{\nu t}$ corresponds to 0.00767 and 0.02236, respectively. Iso-vorticity lines are shown, vorticity levels are equal in terms of scaled vorticity, $4t\omega$, and start from ± 25 and are spaced 25 units apart. The small grid shown on the lower-right side of both parts corresponds to the numerical grid drawn with double spacing for readability.

the same self-similar solution (for a local Reynolds number $Re_s = 2743$, Luchini & Tognaccini 2002, figure 2*b*) if it were a semi-infinite wedge, but at two different stages of the evolution, and different resolution, in the present orifice flow. Figure 4 shows that despite the different resolution the flow field is quantitatively the same as the cited reference although the later solution (figure 4*b*) shows a small influence of the symmetric vortex.

The numerical solution of the orifice flow has been preceded by an accuracy verification to assess the required spatial resolution and the domain extension. A final grid refinement control is partly shown in figure 5. The analysis confirmed the validity and robustness of the solution methods and the small sensitivity of the solution with a two-fold variation of the resolution along each coordinate. In the calculation presented below, the finite domain $[-2, +16] \times [-4, 0]$ is reproduced with a grid spacing $\Delta x = \Delta y = 1/64$, resulting in a discrete domain 1153×257 s. The time step has been selected to guarantee the stability conditions; in almost all cases it is taken as $\Delta t = 1/512$.

The numerical simulations have been first performed for the case of an impulsively started flow, $V(t) = 1$, at $Re = 2000$ and $Re = 5000$ (cases 1 and 2) to identify the general solution and to verify the possible dependence on the Reynolds number in this narrow range corresponding to the values commonly encountered across cardiac valves. Then, additional results are reported that correspond to a smoothly growing flow $V(t) = 1 - e^{t/20}$ (case 3), a pulse $V(t) = \sin(t/10)$ (case 4) and continuously growing flow $V(t) = t/4$ (case 5) with a Reynolds number $Re = 5000$ (that actually will correspond to an average Reynolds number smaller than 3000, with the exception of the last case at later times). The specific parameters are chosen, on the basis of the previous analysis, to have profiles quite different among them and from the impulsively started flow, and to identify the common behaviour in correspondence of uncorrelated time profiles $V(t)$.

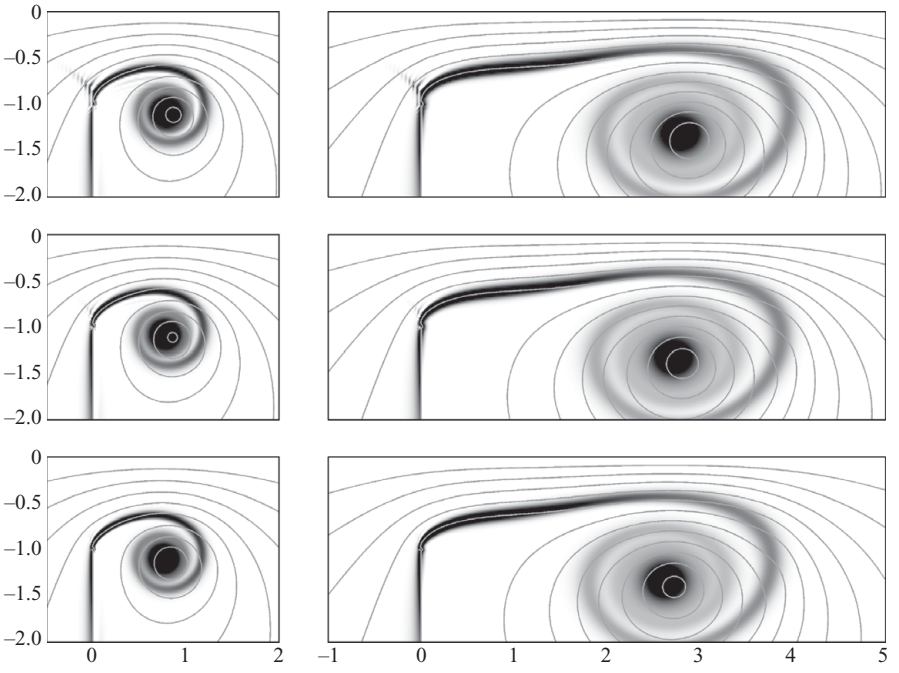

FIGURE 5. Grid refinement study: from top to bottom, comparison between results obtained with resolution results $\Delta x = \Delta y = 1/48, 1/64, 1/96$. Two instants at $t = 1.25$ (left panel) and $t = 3.75$ (right panel) during vortex formation at the exit of a two-dimensional orifice at $Re = 2000$ for an impulsively started flow $V = 1$. Distribution of the vorticity (white is $\omega = 0$, black is $\omega = 8$) and streamlines (streamfunction levels spaced 0.2).

3.2. *Numerical results*

The typical flow evolution is shown in figure 6 for the first case ($V = 1$, $Re = 2000$) at three different times. The vortex dynamics does not present the phenomenon of pinch-off, rather it tends to an apparently stably evolving configuration. In order to better investigate the evolution of the vortex wake, the vertically integrated vorticity, $\Delta v(x, t)$, is computed

$$\Delta v(x, t) = \int_{-\infty}^{0} \omega(x, y, t)\, \mathrm{d}y;$$

this function essentially represents the difference in velocity between above and below the shear layer and vortex structure. The average (vorticity-weighted) velocity, v_ω, of this vortex profile is computed similarly

$$v_\omega(x, t) = \frac{1}{\Delta v(x, t)} \int_{-\infty}^{0} \omega(x, y, t) v_x(x, y, t)\, \mathrm{d}y.$$

The function v_ω corresponding to the vortex layer gives the average velocity of the layer; at the location of the rolled-up vortex structure it measures the translation velocity of the vortex structure.

The space–time maps of these integral quantities are reported in figure 7. Looking at the map of the integrated vorticity (figure 7*a*) it is evident that as the vortex translates downstream, its local intensity Δv remains approximately constant and its longitudinal extension Δx_v grows linearly with the position such that $\Delta x_v / x_v$ remains

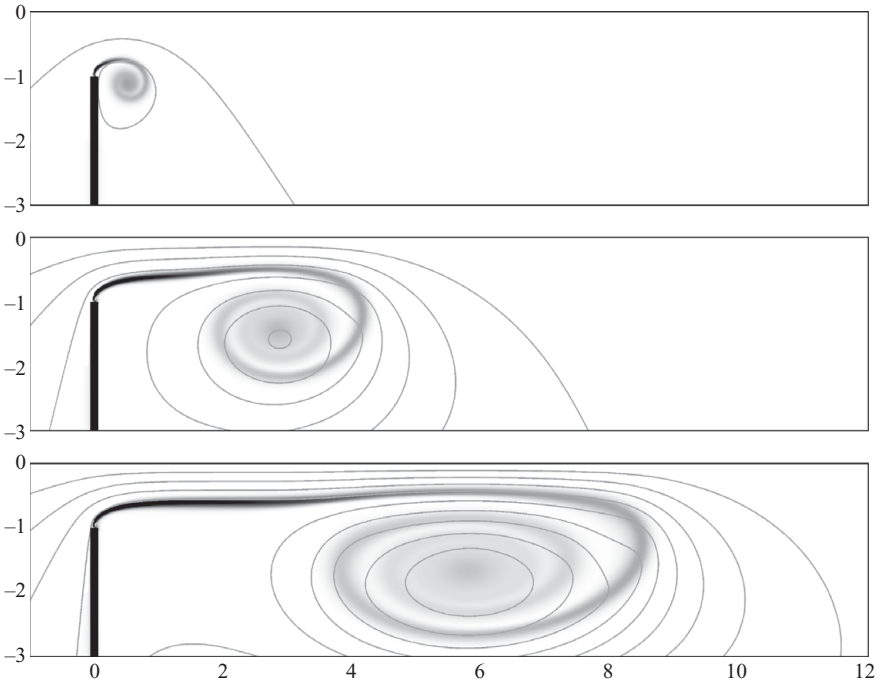

FIGURE 6. Vortex formation at the exit of a two-dimensional orifice at $Re = 2000$ for an impulsively started flow $V = 1$, $t = 2, 10, 20$ ($\tau = 1, 5, 10$). Distribution of the vorticity (white is $\omega = 0$, black is $\omega = 10$) and streamlines (streamfunction levels spaced 0.2).

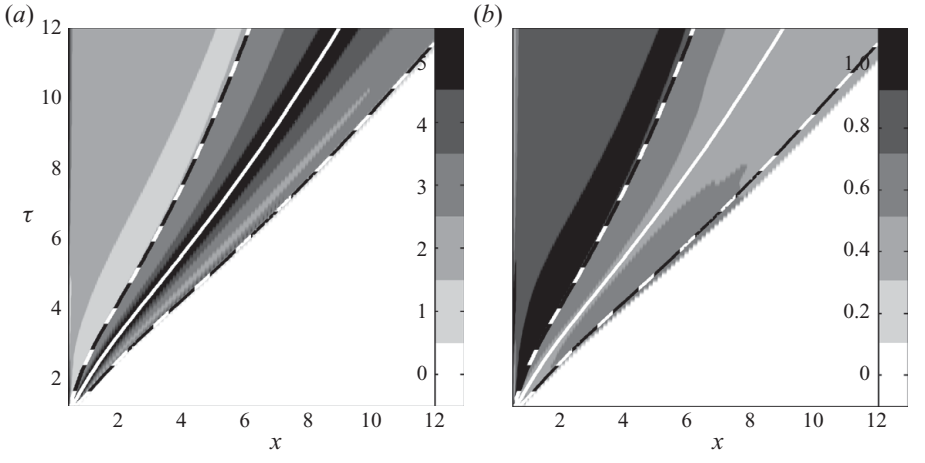

FIGURE 7. Vortex formation at the exit of a two-dimensional orifice at $Re = 2000$ for an impulsively started flow $V = 1$: space–time map of the vertically integrated vorticity, Δv (a), and of the corresponding horizontal velocity, v_ω (b). The continuous line is the automatically detected centre of the separated vortex, the dashed lines are the estimated vortex boundaries.

approximately constant. The shear layer that connects the vortex to the sharp edge also maintains an approximately constant unitary strength. The velocity of the vortex structure (figure 7*b*) also shows that the vortex velocity settles to an approximately constant value, a value that is lower than the speed of the upstream shear layer.

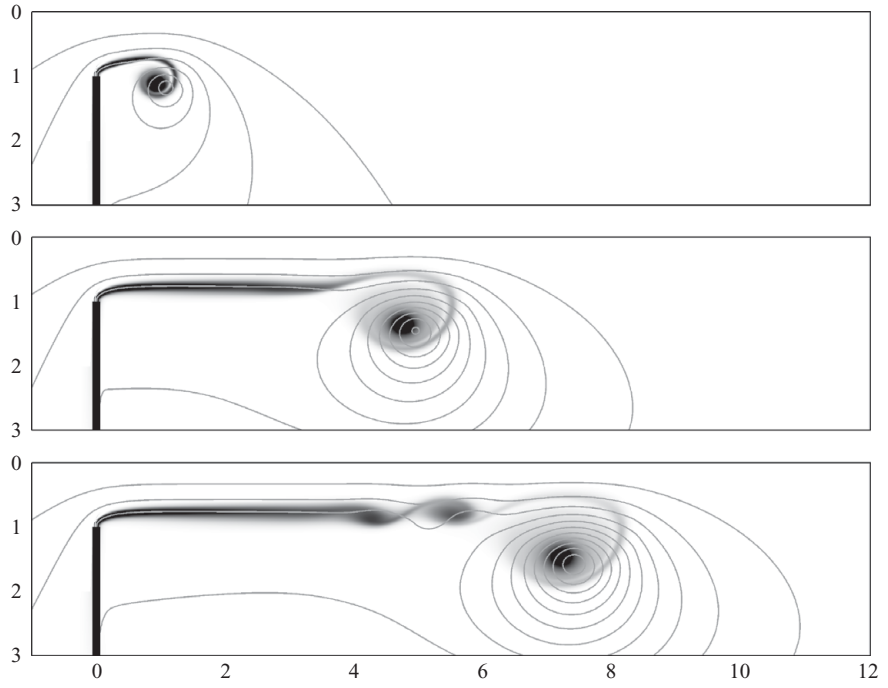

FIGURE 8. Vortex ring formation at the exit of a circular orifice at $Re = 2000$ for an impulsively started flow $V = 1$, $t = 2, 7, 10$ ($\tau = 1, 3.5, 5$). Distribution of the azimuthal vorticity (white is $\omega = 0$, black is $\omega = 10$) and streamlines (Stokes streamfunction levels spaced 0.2).

The evolution does not indicate any tendency of the vortex to accelerate and detach from the separating shear layer (pinch-off). The shear layer is able to continuously feed the vortex with new vorticity, that does not concentrate into the vortex core but contributes to increase the longitudinal finite size of the leading vortex.

In order to better appreciate the difference, the axially symmetric counterpart of this solution is shown in figure 8 that reports the formation of a vortex ring from a circular orifice under identical conditions. This numerical solution is performed with the same numerical code and physical and numerical parameters as those of the two-dimensional case; the only difference is that the axially symmetric versions of the vorticity and Poisson equations are employed, using the Stokes streamfunction and the axisymmetric irrotational basic solution (given, for example, in Lamb 1932, Art. 107–108). The axisymmetric analysis, for which numerous previous studies exist, is also performed as a further validation of the numerical techniques employed. The resulting vortex ring formation perfectly agrees with the existing literature results: a critical formation time exists in the axisymmetric configuration and the critical value is about $\tau \simeq 4$; at that time the leading vortex ring moves away faster than the attached shear layer, and secondary vortices roll-up behind it. Figure 8 shows this phenomenon with the appearance of secondary vortices from $\tau = 3.5$ to $\tau = 5$; during this period the leading vortex ceases to grow (see later in figure 11). This phenomenon was first reported experimentally by Gharib *et al.* (1998, compare with the famous figure 3 therein), demonstrating also that the leading vortex ceases to increase at about $\tau \simeq 4$ (the precise value depending on the definition, and possibly slightly dependent on the specific conditions). After that it was confirmed, with the same critical τ values by other experiments, numerical simulations and observation in nature (see Dabiri 2009, for a recent review).

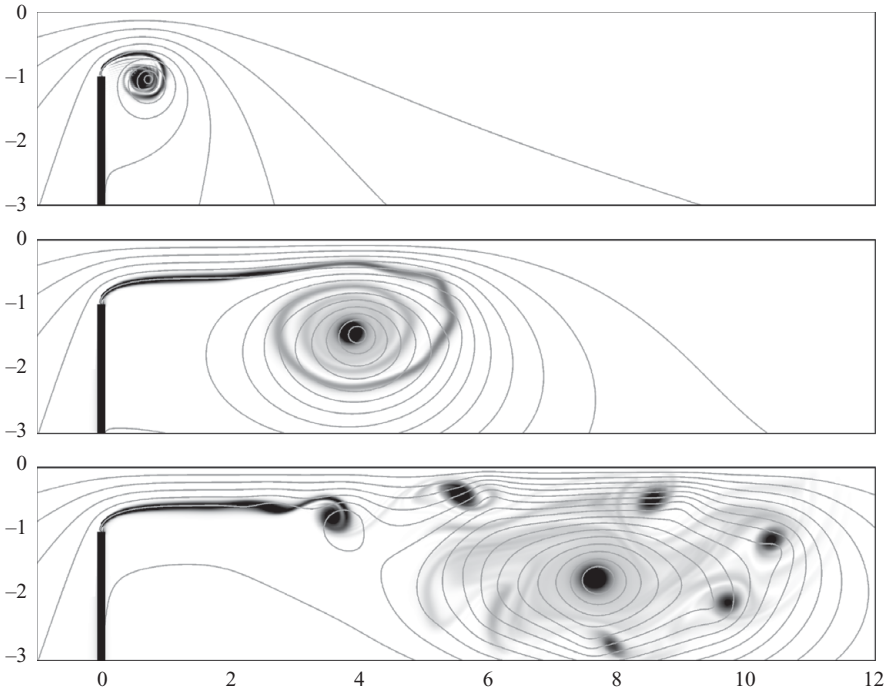

FIGURE 9. Vortex formation at the exit of a two-dimensional orifice at $Re = 5000$ for an impulsively started flow $V = 1$, $t = 2, 10, 20$ ($\tau = 1, 5, 10$). Distribution of the vorticity (white is $\omega = 0$, black is $\omega = 10$) and streamlines (streamfunction levels spaced 0.2).

Comparison between figures 6 and 8 shows that the vortex formation process is substantially slower for two-dimensional vortex pairs. Actually, the very initial phase is analogous in the two systems; the growth of the thin viscous layer with the starting vortex formation at the orifice edge is dominated at the edge by the square root singular character of the irrotational external velocity. The initial vortex formation sharply reduces the local velocity at the edge and at the vortex position as well. After this initial viscosity-ruled period, the local vorticity dynamics enters into play and the evolution of a rectilinear (two-dimensional) vortex differentiates from that of a circular one. The initial two-dimensional vortex dynamics is well approximated by the single vortex model, where (see figure 1) the vortex growth, with a decreasing velocity up to unit time, is analogous to the self-similar formation from a single wedge. Differently, the separating vortex ring immediately presents a significant self-induced velocity due to the curvature of the vorticity lines that leads it always further than the corresponding two-dimensional vortex. Afterwards, the axisymmetric vortex formation arranges into a compact leading vortex ring structure rapidly translating downstream with self-induced velocity, whereas the two-dimensional vortex structure is less compact, probably because vorticity dynamics is not associated with the stretching of vortex lines, and continuously increases its size during formation.

The two-dimensional vortex formation process described earlier does not reveal a tendency towards pinch-off. This is in agreement with the experimental result at Reynolds number of a few hundred (Afanasyev 2006). The behaviour at larger Reynolds number ($Re = 5000$, case 2) is reported in figure 9. The thin shear layer presents the development of an instability (similar to a Kelvin–Helmholtz instability

for a plane vortex sheet) that gives rise to the roll-up of small vortices. Their dynamical interaction is increasingly chaotic and eventually destroys the coherent structure that detaches from the shear layer behind. However, this phenomenon is different from the pinch-off of a coherent vortex ring (compare with figure 8). The lack of coherence of the vortex formation process is not a consequence of the acceleration of the leading vortex to velocity higher than the shear layer behind: the average velocity of the leading vortex pair is always lower than that. The final result is not a compact vortex ring translating away from the formation region: the leading vorticity distribution is progressively disturbed and eventually incoherent.

The development of such small-scale structures from shear layer instability is the same phenomenon observed during the roll-up of a single vortex from a semi-infinite wedge (Luchini & Tognaccini 2002), where a value about 4500 was suggested as the critical value of the Reynolds number for this instability to develop. In that case, however, the system is unbounded and the solution is self-similar; the Reynolds number is based on the growing vortex size and increases in time as well. In the case of a bounded-symmetric system the orifice length scale imposes an upper bound to the effective Reynolds number. Therefore the growth of perturbations may be influenced by the Reynolds number time variation and the actual critical value may be different in the two cases. Furthermore, the self-induced velocity of the symmetric vortex pair produces a larger and differential stretching of the shear layer which certainly influences its stability properties. The experimental and numerical results reported by Hofmans (1998, chapter 3) in similar conditions at $Re = 5270$ also show the development of a shear layer instability and the progressive incoherence of the vortex pair structure that, in the experiment, becomes three-dimensional and weakly turbulent. Similar results are obtained there with two-dimensional numerical methods based on the Euler equation and small artificial viscous effects (just to allow vortex separation). In all cases reported (Hofmans 1998, chapter 3), the translation velocity of the vortex structure (estimable, from the pictures, as roughly between $V/4$ and $V/6$) remains well below that of the separating shear layer; this is a further confirmation that in those experiments, like in the case of figure 9, the termination of the coherent vortex formation process does not correspond to the pinch-off phenomenon. The Reynolds number dependence on the stability of the two-dimensional vortex formation is reported in the same work in a modified geometry with a slightly diverging orifice duct as a model for vocal folds (Hofmans 1998, chapter 4) where the formation of a stable vortex pair is shown at $Re = 1256$ and the development of multiple vortices at $Re = 4061$.

The coherent vortex formation process in the absence of the shear layer instability, described above for an impulsively started flow at $Re = 2000$, is not modified in the presence of a different flow profile $V(t)$ once the variables are properly normalized. Formation time (2.8) remains the fundamental parameter that defines the time evolution of the system. The velocity of the vortex scales with the external velocity and presents a similar behaviour, as is shown in figure 10 for the five different cases. Some noise in the estimation of the vortex parameters is unavoidable; the vortex centre is taken from the position of the extreme value of the streamfunction, and its velocity after time derivative (with 0.25 time units intervals). The vortex velocity initially decreases like that of an isolated vortex (following (2.10)) then, when the influence of the symmetric vortex enters into play, reaches a minimum at about $\tau \simeq 1$ and begins to accelerate again as suggested by the singular vortex theory. However, while the singular vortex theory gives rise to an unbounded growth, the actual vortex velocity presents a weak temporary growth and then tends to a constant or weakly

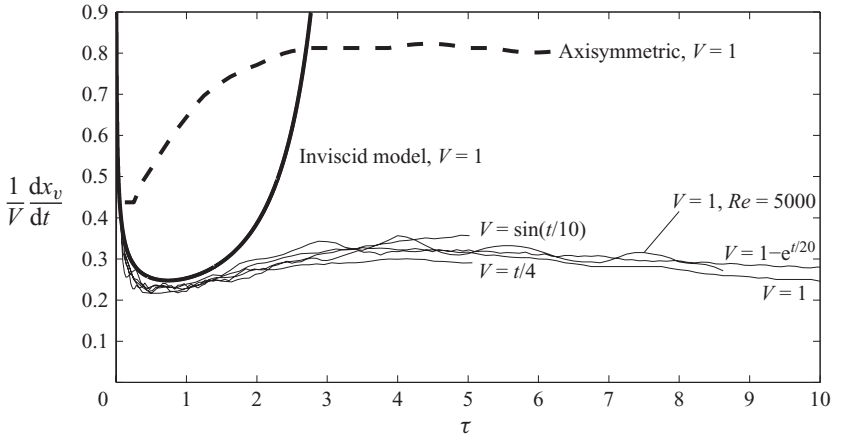

FIGURE 10. Time evolution of the vortex velocity, normalized by the freestream velocity $(1/V)(\mathrm{d}x_v/\mathrm{d}t)$ for the five numerical solutions; the thick line represents the single vortex solution, the thick dashed line is evaluated from the axisymmetric solution.

decreasing (probably because of viscous diffusion) value. The eventual values are comparable to those estimable from the pictures reported in Hofmans (1998). The self-induced velocity is initially that of a vortex-pair then, as the vortex elongates longitudinally, it departs from this and becomes more similar to that of a pair of parallel thick shear layers.

The vortex formation picture, after the initial developing phase, is that of a vortex structure that translates downstream, with velocity proportional to V, increases its longitudinal size, with a rate again proportional to V, attached to and continuously fed by the shear layer connecting it to the sharp edge. The integrated vorticity value (total shear) remains about constant (again proportional to V, neglecting viscous diffusion effects in the discussion), and circulation grows with the vortex size length. The circulation growth is thus given by the intensity of the incoming vortex layer, $\Delta v(x_{\mathrm{layer}})$, times the velocity difference between the vortex layer and the leading vortex pair, $v_\omega(x_{\mathrm{layer}}) - v_\omega(x_v)$:

$$\frac{\mathrm{d}\Gamma}{\mathrm{d}t} = \Delta v(x_{\mathrm{layer}})[v_\omega(x_{\mathrm{layer}}) - v_\omega(x_v)] \simeq 2V\frac{V}{2} = V^2. \tag{3.2}$$

In order to verify this picture the vortex circulation is estimated by integrating the velocity difference $\Delta v(x, t)$ between the edges of the vortex (x_{v_1} and x_{v_2}, estimated by the position of the extreme Δv gradients) and taking its time derivative. Figure 11 reports the evolution of $\mathrm{d}\Gamma/\mathrm{d}t$, normalized with V^2, for the five different cases. Inaccuracies at small times are due to the difficulty in properly identifying the vortex boundaries, a problem also arising later for the case 2 ($Re = 5000$) after the development of the shear layer instability, and for the axisymmetric case during the development of trailing vortices. Despite these, the graph shows quantitative evidence of scaling (3.2) and supports the overall observed picture of the two-dimensional vortex formation without pinch-off. In the axisymmetric case, on the contrary, the leading vortex circulation tends to stop growing after the critical formation time. For completeness, it should be mentioned that scalings reported here implicitly assume that the external flow does not decelerate and does not present abrupt variation.

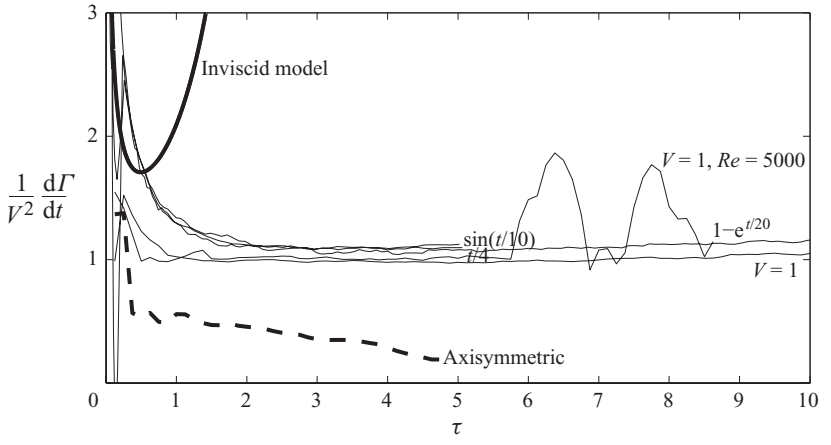

FIGURE 11. Time evolution of the vortex circulation growth, normalized by the squared freestream velocity $(1/V^2)(d\Gamma/dt)$ for the five numerical solutions; the thick line represents the single vortex solution, the thick dashed line is evaluated from the axisymmetric solution.

Otherwise, the development of a spatially varying intensity of the shear layer may give rise to different phenomena not accounted in the present discussion.

4. Conclusions

The formation process of a vortex pair is studied in two-dimensional flow after a sharp orifice. The analysis has been first performed in the inviscid limit with a symmetric single-vortex model that is an approximation for the early stage of the formation process, while the vortex structure is a nearly circular spiralling vortex sheet. In this simplified framework, the evolutionary equation can be written in self-similar terms, independently from the external velocity profile, and the formation time naturally arises as the fundamental quantity to describe the timing of the vortex formation (Gharib *et al.* 1998). The early formation stage shows that the vortex pair initially grows as two independent vortices, and then accelerates because of the self-induced velocity. This model also allows the obtaining of explicit evidence for the influence of the geometry on the timing of the vortex formation process; an influence that is small or negligible in the axially symmetric formation of vortex rings (Rosenfeld *et al.* 1998).

The analysis in the presence of a spatially extended vortex structure has been prosecuted by numerical simulations of the two-dimensional Navier–Stokes equations. The results do not show any evidence of the pinch-off phenomenon previously reported in the formation of axially symmetric vortex rings. The vortex pair tends to a stably growing evolution: it translates downstream, extends longitudinally and remains connected to the sharp edge by a vortex layer whose velocity is always about twice that of the leading vortex. The incoming shear layer continuously feeds the vortex with new vorticity that does not accumulate in the vortex centre but increases the vortex circulation by increasing its longitudinal extension only. Although the circulation grows in time, the self-induced velocity of the vortex pair is bounded because it progressively becomes that of a pair of parallel shear layers with intensity proportional to the external velocity.

This result, found for Reynolds numbers of a few thousand, is in agreement with an existing experimental study at Reynolds numbers of a few hundred. When

the Reynolds number exceeds a limit value the separating shear layer becomes unstable and develops small vortices from its local roll-up. The critical Re value (roughly somewhat below 5000, but it may also depend on the velocity profile and orifice geometry) is comparable with the critical value $Re = 4500$, previously estimated for the roll-up of a single shear layer (Luchini & Tognaccini 2002). These small-scale structures progressively break the coherence of the leading vortex pair that eventually detaches from the formation edge. This phenomenon was previously observed in the experimental results by Hofmans (1998). Following the present and the Hofmans' results, the two-dimensional instability of vortex formation is a different phenomenon than the pinch-off of vortex rings; the average velocity of the leading vortex structure remains below that of the incoming vortex layer, and becomes progressively incoherent.

This work indicates that, differently from the axially symmetric case, a critical formation time cannot be defined for two-dimensional vortex formation after orifices. The qualitatively different behaviour between the formation of vortex rings (pinch-off) and two-dimensional vortex pairs (stable growth, or instability at larger Re) suggests multiple possibilities in the formation of three-dimensional vortex structures from orifices with variable curvature or with a tapered mouth.

The author is grateful to Professor A. Kheradvar for useful suggestions, and to Professor J. O. Dabiri for a relevant reference. The author is also grateful to an anonymous referee for the reference of existing experimental results.

REFERENCES

Afanasyev, Y. D. 2006 Formation of vortex dipoles. *Phys. Fluids* **18**, 037103.

Blondeaux, P. & De Bernardinis, B. 1983 On the formation of vortex pairs near orifices. *J. Fluid Mech.* **135**, 111–122.

Brown, C. E. & Michael, W. H. 1954 Effect of leading edge separation on the lift of a delta wing. *J. Aeronaut. Sci.* **21** (10), 690–694, 706.

Dabiri, J. O. 2009 Optimal vortex formation as a unifying principle in biological propulsion. *Annu. Rev. Fluid Mech.* **41**, 17–33.

Dabiri, J. O. & Gharib, M. 2005 Starting flow through nozzles with temporally variable exit diameter. *J. Fluid Mech.* **538**, 111–136.

Gharib, M., Rambod, E., Kheradvar, A., Sahn, D. J. & Dabiri, J. O. 2006 Optimal vortex formation as an index of cardiac health. *Proc. Natl Acad. Sci.* **109**, 6205–6308.

Gharib, M., Rambod, E. & Shariff, K. 1998 A universal time scale for vortex ring formation. *J. Fluid Mech.* **360**, 121–140.

Hofmans, G. C. J. 1998 *Vortex Sound in Confined Flows*. Technische Universiteit Eindhoven. ISBN 90-386-0697-4. http://alexandria.tue.nl/extra2/9802719.pdf.

Hong, G. R., Pedrizzetti, G., Tonti, G., Li, P., Wei, P., Kim, J. K., Bawela, A., Liu, S., Chung, N., Houle, H., Narula, J. & Vannan, M. A. 2008 Characterization and quantification of vortex flow in the human left ventricle. *J. Am. Coll. Cardiol. Img.* **1**, 705–717.

Kheradvar, A. & Gharib, M. 2007 Influence of ventricular pressure drop on mitral annulus dynamics through the process of vortex ring formation. *Ann. Biomed. Engng* **35**, 2050–2064.

Kheradvar, A. & Gharib, M. 2009 On mitral valve dynamics and its connection to early diastolic flow. *Ann. Biomed. Engng* **37**, 1–13.

Kilner, P. J., Yang, G. Z., Wilkes, A. J., Mohiaddin, R. H., Firmin, D. N. & Yacoub, M. H. 2000 Asymmetric redirection of flow through the heart. *Nature* **404**, 759–761.

Korakianitis, T. & Shi, Y. 2006 Numerical simulation of cardiovascular dynamics with healthy and diseased heart valves. *J. Biomech.* **39**, 1964–1982.

Krueger, P. S. 2008 Circulation and trajectories of vortex rings formed from tube and orifice openings. *Physica* D **237**, 2218–2222.

Lamb, H. 1932. *Hydrodynamics*, 6th edn. Cambridge University Press.

Luchini, P. & Tognaccini, R. 2002 The start-up vortex issuing from a semi-infinite flat plate. *J. Fluid Mech.* **455**, 175–193.

Mohseni, K. & Gharib, M. 1998 A model for universal time scale of vortex ring formation. *Phys. Fluids* **10**, 2436–2438.

Mohseni, K., Ran, H. Y. & Colonius, T. 2001 Numerical experiments on vortex ring formation. *J. Fluid Mech.* **430**, 267–282.

Pedrizzetti, G. 2005 Kinematic characterization of valvular opening. *Phys. Rev. Lett.* **94**, 194–502.

Pedrizzetti, G. & Domenichini, F. 2005 Nature optimizes the swirling flow in the human left ventricle. *Phys. Rev. Lett.* **95**, 1080101.

Pedrizzetti, G. & Domenichini, F. 2006 Flow-driven opening of a valvular leaflet. *J. Fluid Mech.* **569**, 321–330.

Pedrizzetti, G. & Domenichini, F. 2007 Asymmetric opening of a simple bi-leaflet valve. *Phys. Rev. Lett.* **98**, 214–503.

Pullin, D. I. 1978 The large-scale structure of unsteady self-similar rolled-up vortex sheets. *J. Fluid Mech.* **88**, 401–430.

Rosenfeld, M., Rambod, E. & Gharib, M. 1998 Circulation and formation number of laminar vortex rings. *J. Fluid Mech.* **376**, 297–318.

Rott, N. 1956 Diffraction of a weak shock with vortex generation. *J. Fluid Mech.* **1**, 111–128.

Routh, E. J. 1881 Some applications of conjugate functions *Proc. Lond. Math. Soc.* **12**, 73–89.

Shusser, M. & Gharib, M. 2000 Energy and velocity of a forming vortex ring. *Phys. Fluids* **12**, 618–621.